Supporting Information: Physical interactions tune the chemisorption of polar anions on carbon nanostructures

A. Hasmy,*,†,‡ L. C. Rincón,¶ A. Noury,‡ F. Henn,‡ and V. Jourdain‡

†*Departamento de Física, Universidad Simón Bolívar, Valle de Sartenejas, 1080 Caracas, Venezuela*

‡*Laboratoire Charles Coulomb, Univ Montpellier, CNRS, Montpellier, France*

¶*Grupo de Química Computacional y Teórica and Instituto de Simulación Computacional, Universidad San Francisco de Quito, Quito 170901, Ecuador*

E-mail: anwarhasmy@hotmail.com

S1. Initial configurations

For the anion adsorption on carbon nanostructures, we use a supercell of dimension (L_x, L_y, L_z), where $L_y \simeq L_x$ for graphene, and $L_y = L_z$ for SWCNTs, where x and z correspond to the tube axis and the bonding axis direction, respectively. To reduce finite size effects, we have considered Periodic Boundary Conditions (PBC) in all our samples, taking into account that the SWCNT and graphene edges must be coupled with their images.

Our study includes calculations on metallic M-armchair (n,n) and M-zigzag, and semiconducting SC-zigzag (n,0) SWCNTs as well some M- and SC-chiral (n,m) SWCNTs were considered. Then, the number of atoms, and therefore the supercell sizes, were chosen small enough to speed up the calculations, but as large as necessary to well reproduce the results whatever the supercell size. An optimum size is obtained by analyzing the total density of states (DOS) of pristine carbon nanostructures of different sizes. We have

found that CNTs longer than 1.7 nm reduce oscillations and ensure a good convergence in the total DOS (see Fig. S1).

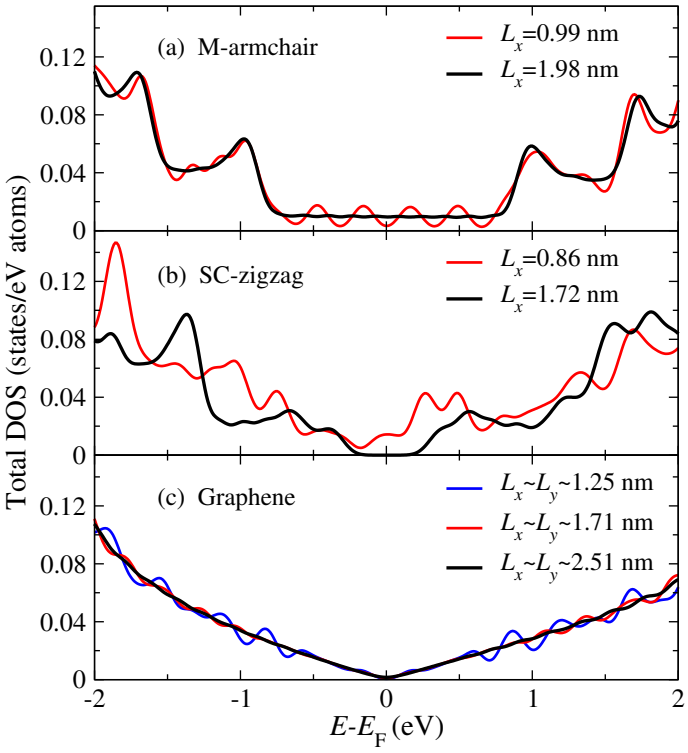

FIG. S1: Total DOS respect to the Fermi level of pristine M-armchair (8,8) and SC-zigzag (14,0) SWCNTs of different lengths (number of unit cells), and graphene of different sizes. The calculations include periodic boundary conditions.

We considered tube diameters between 0.6 and 3.0 nm (128 and 824 C atoms), and the smallest tube length L_x used here was equal to 1.71 nm. For M-armchair (n,n) SWCNTs, we used 8 unit cells with n equal to 5, 8, 10, 11, 12, 14, 18 and 22. For zigzag (n,0) SWCNTs, we used 4 unit cells, with n=9,12,18,24,30 for M-zigzag tubes, and n=8,14,17,19,25 for SC-zigzag ones. For M-chiral (n,m) tubes we considered n=12, with m=3,6,9, and n = 18 with m =6,12, and (11,5). For SC-chiral we included (12,4) and (18,4) CNTs. In chiral tubes the number of unit cells varied depending on the chiral angle. A graphene sheet of 240 C atoms was also included for comparison.

S2. Electronic structure calculations

For the electronic structure calculations we have implemented the SCC-DFTB method for the electronic structure calculations.[1] This method has been proven to be as accurate as

DFT methods but three orders of magnitude faster .[2–7] In particular we implemented the DFTB3 approximation, which includes a third-order expansion of the Kohn-Sham total energy in Density-Functional Theory (DFT) with respect to charge density fluctuations.[8] We used the Slater-Koster parameters denoted 3ob, which correspond to the state-of-the-art of the DFTB parametrization obtained by fitting their thermochemistry, geometrical and vibrational properties on a variety of organic molecules.[8] The gamma point is used in the K-point sampling of the first Brillouin zone of the supercell, and for the calculations of the Density of States (DOS), we have used 10x10x1 K-points mesh for graphene and 10x1x1 for SC-SWCNTs.

S3. Energy profiles

The geometry of the pristine graphene and SWCNTs are optimized by combining the SCC-DFTB method with the Limited-memory Broyden Fletcher Goldfarb Shanno (L-BFGS) technique.[9] We have allowed changes to the lattice vectors of the supercell in the directions where the sample edges match their images. Then, the positions of O and it closest C_0 atom anion are fixed at a distance d_{SA}, while the other atoms are again fully relaxed as explained in the main text. To evaluate the energy profiles using Eq. (1) of the main text, we point out that $d_{OH-K} = L_Z/2 - d_{SA} - R$, where R is the tube radius. For the E_C and E_{OH-K} estimations, the supercell size is similar to that used for the whole sample calculations. A supercell length $L_Z = 100$ Å has been used to reduce the counterion effects on the energy profiles (see Fig. S2a).

To asses the more favorable site for the OH^- adsorption on the carbon surface, we explore the anion binding on three potential sites of high symmetry: the top (Top) site where the O atom faces the C_0 atom, the hollow (Hol) site where the O atom is equally distant from the 6 C atoms of the hexagon and the bridge (Bri) site where it is at the midpoint above a C-C bond. The number of C atoms fixed around the adsorption region is one, two and three, respectively. Fig. S2b shows that a strong adsorption state only appears when the exohedral adsorption occurs at Top sites. All results shown in the main text focus on the adsorption at the Top symmetry, therefore in this study the distance

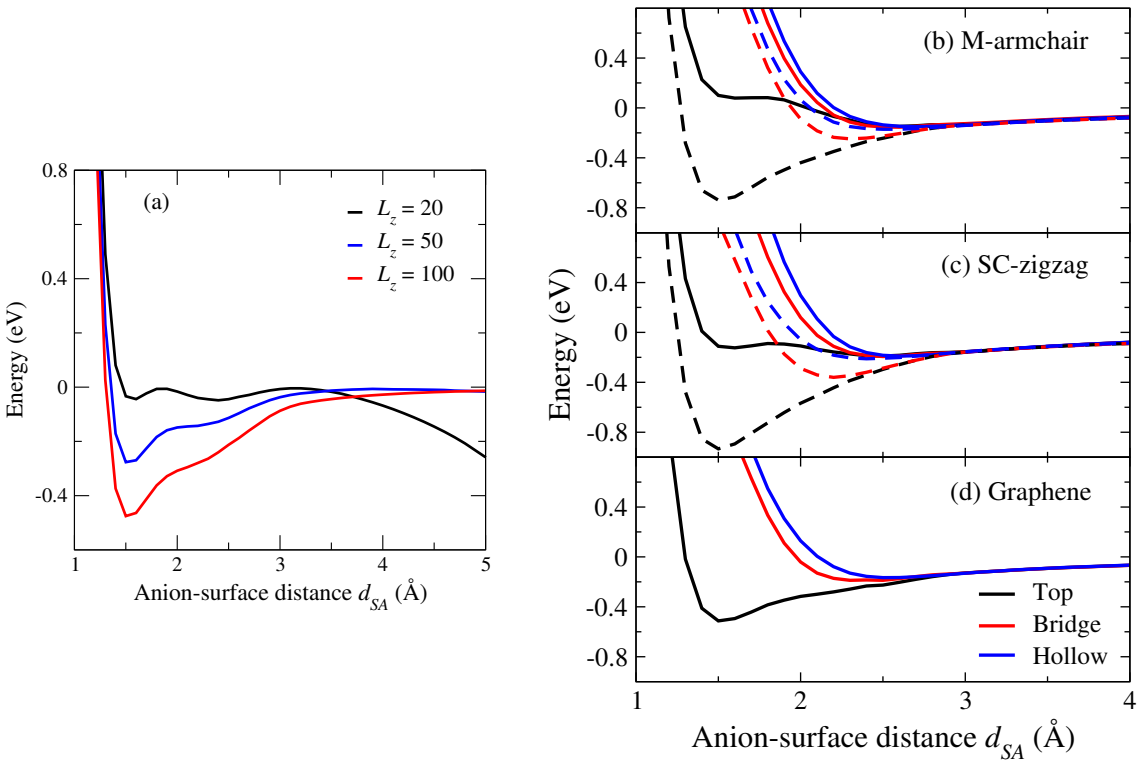

Fig S2: Energy profiles for the OH^- adsorption on: (a) graphene of different length sizes L_z of the supercell at the Top binding symmetry. The counterion K^+ is located at a distance of $L_z/2$ from the tube axis. (b-d) graphene and SWCNTs of 1.1-nm for different adsorption binding site symmetries (Hollow, Top, Bridge) and $L_z = 100$. The solid and dashed curves correspond to endo- and exohedral adsorption, respectively.

d_{SA} defines the distance between the O atom and its nearest carbon atom C_0.

To build the energy profiles, the distance d_{SA} was varied by 0.1 Å in a range of 1-5 Å in most of the cases. However, to improve the resolution, once we have identified the energy minima and equlibrium distances d_{SA} in the profiles, we optimize the structure again at the shortest equilibrium distance, but now with the O and C_0 atoms no longer held fixed. Note that such distance is equivalent to the O-C_0 bond length at the energy global minimum.

For OH^- adsorption, the energy profiles on M-armchair, M-zigzag and SC-zigzag tubes are shown in Fig. 1 of the main text. Fig. S3a shows the energy profiles for the chirality familiy (12,3l), varying l from 0 to 4 (note that this family includes M-zigzag, M-chiral and M-armchair tubes). Fig. S3b includes the energy profiles for other M- and SC-chiral tubes.

Figs. S3c and S3d correspond to the energy profiles of the adsorption of SH^-, ClO^-

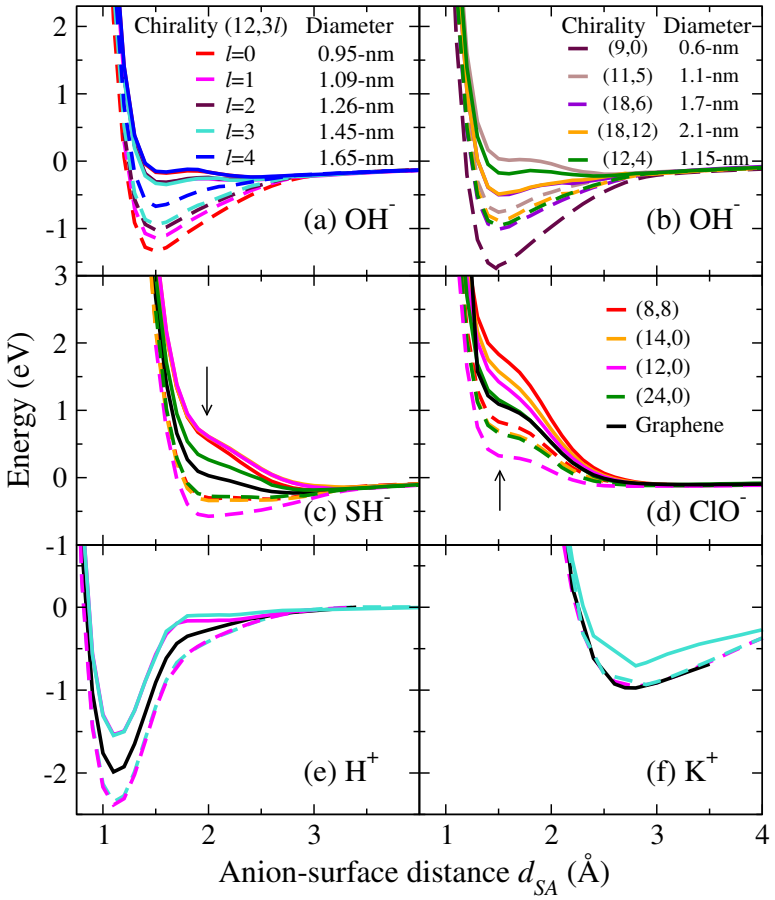

FIG. S3: Energy profiles for the adsorption of (a) OH^- on (12,3l) SWCNTs (l=0,...,4), and (b) on M- and SC-chiral nanotubes. For the adsorption of (c) SH^-, (d) ClO^- (e) H^+, and (f) K^+, on different SWCNTs. The graphene case is included for comparison. Solid and dashed lines correspond to endo- and exohedral adsorption, respectively. The arrows in Figs (c)(d) indicate the unstable states.

on M-armchair, M-zigzag and SC-zigzag SWCNTs with different diameters. In both cases we have found an energy minimum around $d_{SA} \sim 3$ Å. Figs. S3c,d evidence that at lower d_{SA} a stable minimum only appears for SH^- exohedral adsorption. In the other situations, an energy shoulder appears at 2 and 1.5 Å for SH^- and ClO^-, respectively (see the arrows in Figs. S3c,d). The energy shoulder in the energy profiles correspond to unstable states, which we have also estimated by determining the lower slope in the curves at shorter distances. The results are also included in Fig. 3 of the main text.

For comparison, we also calculated the energy profiles of the adsorption of monovalent cations such as H^+ and K^+ on the carbon surfaces. For both cases it has been shown that the interactions with the carbon surface are of chemical nature, being predominately covalent and ionic (metallic) in the former and the latter, respectively, and

no additional physisorption state has been reported.[10,11] Our results are in agreements with these findings (see Fig. S3e,f).

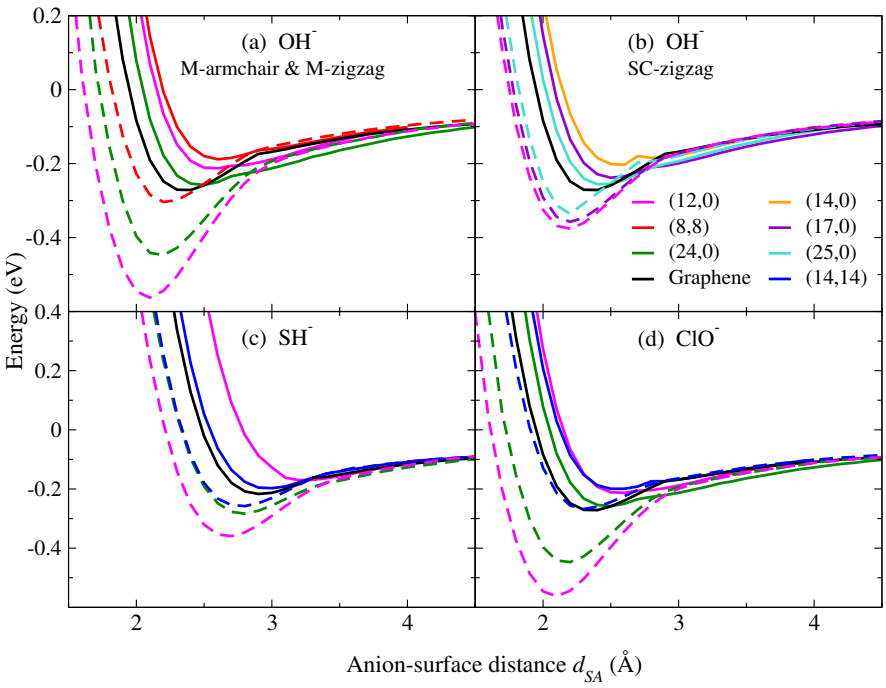

Fig. S4: Energy profiles of undistorted SWCNTs: (a) OH^- adsorption on M-armchair and M-zigzag tubes, and (b) SC-zigzag tubes. (c) SH^- and (d) ClO^- on M-armchair and M-zigzag tube. Solid and dashed curves correspond to endohedral and exohedral adsorption, respectively. The graphene case is included for comparison. The minimum energies correspond to the binding energy denoted as E_{B_2}.

We have also performed energy profile calculations by avoiding any carbon surface deformation originating from chemical interactions with the anions, by fixing all C atoms as for O (or S) and C_0 atoms. Only H (or Cl) are allowed to move during the structure optimization. Figure S4 shows some energy profiles of (a,b) OH^-, (c) SH^- and (d) ClO^-, when the protrusion of the C_0 atom is forbidden (undistorted tube) for different diameters and chiralities. As discussed in the main text, only the physisorption state appears at longer distances ($2 < d_{SA} < 3$ Å). The energy minimum dominated by physical interactions becomes clearly visible in frozen CNT profiles, including the situation when no energy barrier separate it from the chemisorption state in the relaxed CNT profiles (i.e. exohedral adsorption).

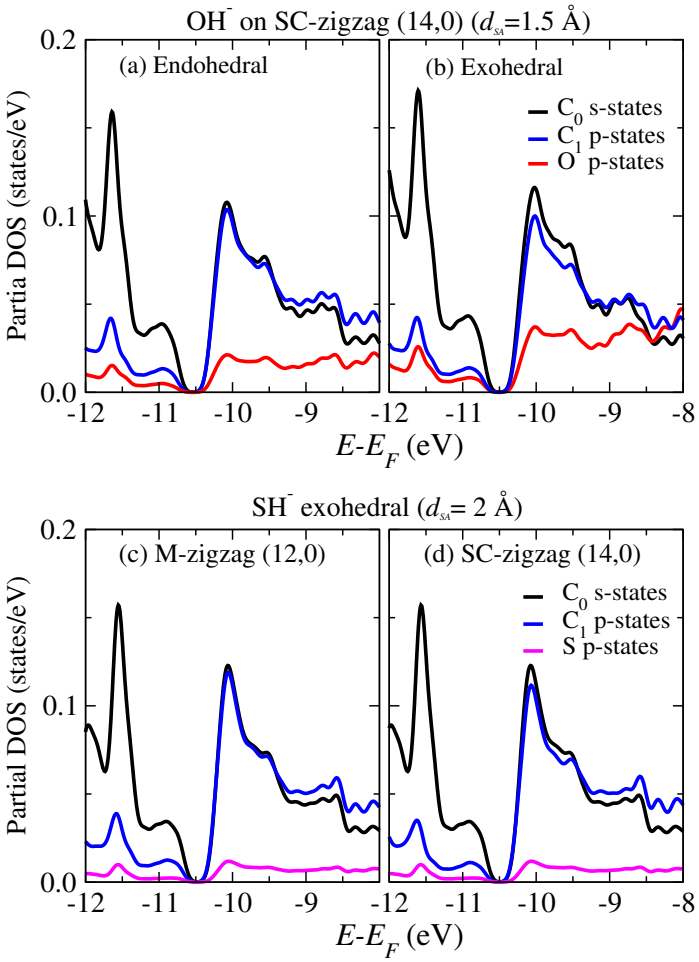

Fig. S5: Partial DOS of the s-states of the C_0 atom and the p-states of it adjacent C_1 and O atoms, for SC-zigzag SWCNTs of 1.1-nm diameter, for (a) endohedral and (b) exohedral adsorption of OH^- at d_{SA} =1.5 Å. (c) and (d) correspond to the partial DOS of SH^- exohedral adsorption on M-zigzag and M-armchair CNTs of 0.95-nm and 1.1-nm diameter, respectively, at d_{SA} =2 Å.

S4. Density of states

Fig. S5 shows the projected DOS for (a) endohedral and (b) exohedral adsorption of OH^- on SC-zigzag SWCNTs of 1.1-nm diameter at d_{SA} =1.5 Å. Fig. 3 of the main text show the corresponding DOS of OH^- adsorbed on M-armchair and M-chiral CNTs. Black and blue curves correspond to the s- and p-states of C_0 and C_1 atoms, and red curve to the p-states of O. All cases exhibit a hybridization between the s-states of C_0 and the p-states of it adjacent C_1 and O atoms, as revealed from the partial overlaps of the curves. This validates the chemical character of the bonding.

Figs S5 (c) and (b) correspond to the projected DOS of SH^- exohedral adsorption on M-zigzag and M-armchair tubes of 0.95-nm and 1.1-nm diameters, respectively. In this

case the hybridisation of the S p-states with the C_0 s-states is much weaker for SH^- than that of OH^-, which is consistent with the lower charge transfer from S to C_0 observed in Fig. 2 of the main text.

S5. Linear dependence of the adsorption energies with surface curvature

Table S1 reports results corresponding to the computed linear regressions of the binding energies versus the tube curvature $(1/R)$. Table S2 shows results corresponding to the different anions obtained from the NIST database.[12]

Table S1: E_0 and the slope A for different anions and nanotubes obtained from linear regressions of the E_{B_1} and E_{B_2} curves in Figs. 3 and 7c of the main text.

	E_{B_1}						E_{B_2}					
	M-armchair		SC-zigzag		M-zigzag		M-armchair		SC-zigzag		M-zigzag	
Anion	E_0(eV)	A (eVÅ)	E_0(eV)	A (eVÅ)	E_0(eV)	A (eVÅ)	E_0(eV)	A (eVÅ)	E_0(eV)	A (eVÅ)	E_0(eV)	A (eVÅ)
OH^-	0.39	2.15	0.60	2.12	0.81	2.44	0.24	0.38	0.30	0.51	0.37	0.88
SH^-	-0.10	2.42	-		-0.11	2.65	-		-		0.25	0.44
ClO^-	-1.33	2.83	-		-0.86	2.83	-		0.04	0.02	0.004	0.02

Table S2: Mulliken atomic charges, dipole moment and polarizability for OH^-, SH^- and ClO^-, and the electronegativity difference for their radicals.

Anion atoms	O	H	S	H	Cl	O
Mulliken atomic charges (e)[a]	-0.75 -1.20	-0.25 +0.20	-0.75 -0.96	-0.25 -0.04	-0.55 -0.26	-0.45 -0.74
Mulliken charges (e) with DFTB+[b]	-0.75	+0.34	-0.42	0.16	-0.12	-0.21
Dipole moment (D)[a]	0.20 0.65		0.20 0.65		1.1 2.6	
Isotropic polarizability (Å^3)[a]	0.26 0.65		0.46 1.40		0.62 1.80	
Electronegativity difference (Pauling scale)[c]	1.24		0.38		0.28	

[a] For isolated anions. Top values correspond to DFT data obtained using STO-3G basis sets. Bottom values corresponds to data with larger basis sets at the DFT, Moller Plesset perturbation or Coupled Cluster level according to the data avalaibility at Ref. [14]

[b] Calculated with 3ob parameter set [1] in presence of the counterion and the CNT, but separated by a distance larger than 4 Å with CNT and 30 Å for the counterion.

[c] For isolated radicals.

S6. Bond lengths

For the OH^- adsorption, Fig. S6a plots the bond length $a_{C_0C_1}$, averaged over the three adjacents C_1 atoms, as a function of the distance d_{SA}, for M-zigzag CNTs of 1.1-nm and 1.9-nm diameter. The graphene case is also included for comparison. In this figure, solid and dashed curves correspond to endo- and exohedral adsorption, respectively. The C_0-C_1 bond length $a_{C_0C_1}$ increases from $1.42-1.43$ to 1.50-1.53 Å as the distance d_{SA} is decreased from the physisorbed state ($d_{SA} \sim 2.5$ Å), to the chemisorbed one ($d_{SA} \sim 1.5$ Å) as highlighted by the arrows in Fig. S6a.

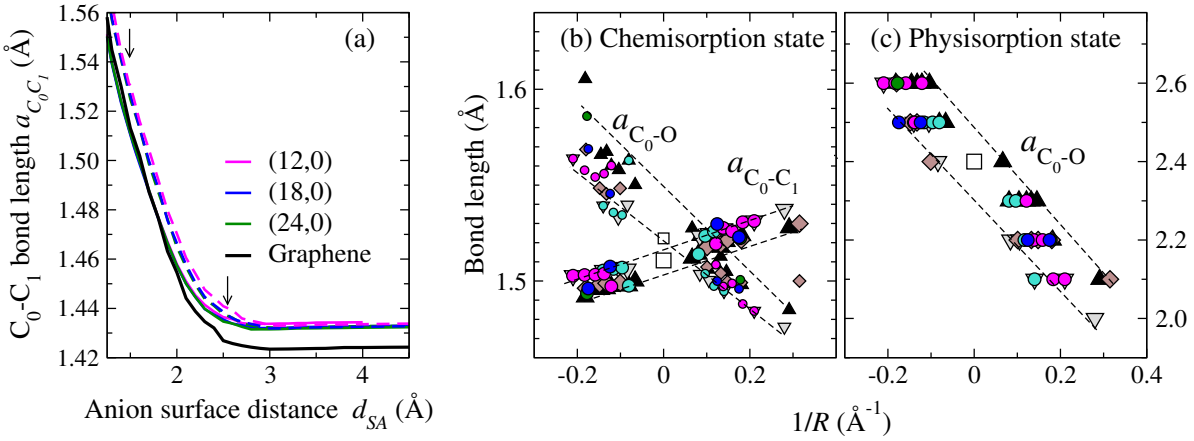

Fig. S6: (a) average bond length $a_{C_0C_1}$ versus the distance d_{SA} for OH^- on M-zigzag tubes (the arrows indicate the chemisorption and physisorption states), (b) the bond lengths $a_{C_0C_1}$ and a_{C_0O} at $d_{SA} \sim 1.5$ Å, and (c) a_{C_0O} at $d_{SA} \sim 2.5$ Å, as a function of the tube curvature $(1/R)$. In (a), solid and dashed lines correspond to endo and exohedral adsorption, respectively. In (b) and (c), the symbols correspond to M-armchair (black triangles), M-zigzag (grey triangles), SC-zigzag (brown diamonds), SC-chiral (blue circles) and M-chiral (magenta, turquoise and green circles) nanotubes, and graphene (open squares). The dashed lines are guides to the eyes to highlight the monotonic increase and decrease with the tube curvature of $a_{C_0C_1}$ and a_{C_0O}, respectively.

For the chemisorption state, Figs. 6 (b) and (c) show the $a_{C_0C_1}$ and O-C_0 bond lengths a_{C_0O}, respectively (defined as the equilibrium distance d_{SA} where the energy profiles exhibit energy minima), as a function of the carbon surface curvature $1/R$ for all CNT samples. The results reveal that the larger the curvature, the larger is $a_{C_0C_1}$ and the smaller is a_{C_0O}. Furthermore, the narrower is the tube, the smaller and the larger is $a_{C_0C_1}$ in the endo- and exohedral case, respectively. The opposite occurs for a_{C_0O} (Fig. S6). The latter is also confirmed for the physisorption state as shown in Fig. S6c.

The dashed lines highlight these tendencies. Similar trends are observed for the stable exohedral adsorption of SH^- on carbon surfaces. In Fig. S6c the resolution for the bond lengths is ± 0.1 Å, which is related to the d_{SA} variation when the energy is minimised in the physisorption state.

S7. Dipole moments

For OH^- and CNTs, we have calculated the dipole moments μ using the Mulliken atomic charges and the expression $\vec{\mu} = \sum_{i=1}^{N} q_i \vec{r_i}$, where the sum runs over all C atoms for the tubes, q_i denotes their charges and $\vec{r_i}$ their positions with respect to the center of mass of the CNT, which is located at the intersection of the tube and bonding axes. Following a similar procedure, we have also calculated the OH^- dipole moment. We have excluded the periodic boundary conditions, and for symmetry reasons we only include those CNTs whose length $L_x \sim 2$ nm, which excludes the chiral tube families ($m, n > 0$ and $m \neq n$) considered in this work. In addition, due to the symmetry of the system, the dipole moments μ_{xy} in the xy-plane and μ_z along the O-C_0 bond axis were estimated separately. Figs. S7a,b show these dipole moments for M-zigzag CNTs of different diameters and for OH^- (with respect to the CNT coordinates), as a function of d_{SA}. The arrows indicate the two adsorption states. The results show that for $d_{SA} < 3$ Å, μ_{xy} of CNTs increases with decreasing d_{SA} from 3 Å, while for OH^- it reaches a maximum at $d_{SA} \sim 2.5$ Å. The opposite occurs for μ_z, i.e., it reaches a maximum for CNTs at that distance, while for the OH^- it disappears for $d_{SA} < 3$ Å. The latter evidences that the orientation of the OH^- dipole moment changes from being perpendicular to the xy-plane to being parallel. Figs. S7c,d shows that μ_{xy} and μ_z scale quadratically with the tube radius R at $d_{SA} = 2.5$ (colored symbols) and 1.5 Å, in agreement with previous works.[13–15] The figures also show that μ_z dominates over μ_{xy} in the physisorption state, while the opposite occurs in the chemisorption state, which may be associated with charge transfer.

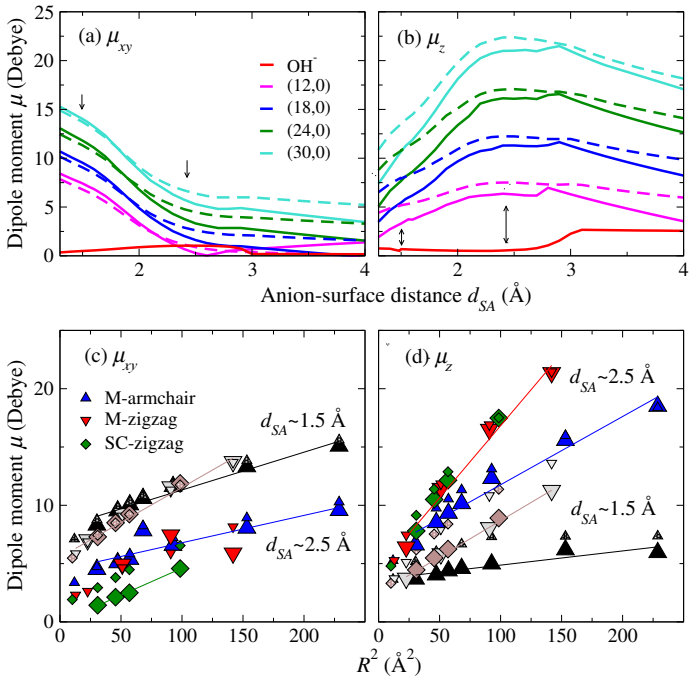

Fig. S7: Dipole moments μ_{xy} and μ_z of OH^- and CNTs as a function of (a,b) the distance d_{SA} and (c,d) R^2 (R is the nanotube radius). In (a) and (b) the arrows denote the equilibrium distances for chemisorption and physisorption. In (c) and (d) small and big symbols correspond to exo- and endohedral adsorption, respectively, colored symbols to the physisorption state, uncolored ones (i.e. black, grey and brown) to chemisorption, and solid lines to linear regressions.

References

(1) Aradi, B.; Hourahine, B.; Frauenheim, T. DFTB+, a sparse matrix-based implementation of the DFTB method. J. Phys. Chem. A **2007**, 111, 5678–5684.

(2) Peralta-Inga, Z.; Boyd, S.; Murray J. S.; O Connor, C. J.; Politzer, P. Density Functional Tight-Binding studies of carbon nanotube Structures. Struct. Chem. **2003**, 14, 431–443.

(3) Rincón, L.; Almeida, R.; González, C. A. On the charge carrier localization in zigzag carbon nanotube junctions. J. Phys. Chem. C **2011**, 115, 11727–11733.

(4) Zobelli, A. *et al.*. A comparative study of density functional and density functional tight binding calculations of defects in graphene. Phys. Stat. Solidi B **2012**, 249, 276–282.

(5) Seo, K.; Park, K. A.; Kim, C.; Han, S.; Kim, B.; Lee, Y. H. Chirality- and diameter-

dependent reactivity of NO_2 on carbon nanotube walls. J. Am. Chem. Soc. **2005**, 127, 15724–15729.

(6) Zheng, G.; Wang, Z.; Irle, S.; Morokuma, K. Origin of the linear relationship between CH_2/NH/O-SWNT reaction energies and sidewall curvature: armchair nanotubes. J. Am. Chem. Soc. **2006**, 128, 15117–15126.

(7) Wang, Z.; Irle, S.; Zheng, G.; Morokuma, K. Analysis of the relationship between reaction energies of electrophilic SWNT additions and sidewall curvature: chiral nanotubes. J. Phys. Chem. C **2008**, 112, 12697–12705.

(8) Gaus, M.; Goez, A.; Elstner, M. Parametrization and benchmark of DFTB3 for Organic Molecules. J. Chem. Theory Comput. **2013**, 9, 1, 338–354.

(9) J. Nocedal and S. J. Wright. "Numerical optimization" (Springer, NY, 2nd ed, 2006).

(10) Liu, Z. H^+ ions on graphene electrode as hydrogen storage reservoirs. Comput. Mater. Sci. **2011**, 50, 3257–3264.

(11) Zhu, C.; Yang, G. Insights from the adsorption of halide Ions on graphene materials. ChemPhysChem **2016**, 17, 2482–2488.

(12) NIST Computational Chemistry Comparison and Benchmark Database, http://cccbdb.nist.gov (2020).

(13) Brothers, E. N.; Kudin, K. N.; Scuseria, G. E. Transverse polarizabilities of carbon nanotubes: A Hartree-Fock and density functional study. Phys. Rev. B **2005**, 72, 033402.

(14) Novikov, D. S.; Levitov, L. S. Energy Anomaly and Polarizability of Carbon Nanotubes. Phys. Rev. Lett. **2006**, 96, 036402.

(15) Kozinsky, B.; Marzari, N. Static dielectric properties of carbon nanotubes from first principles. Phys. Rev. Lett. **2006**, 96, 166801.